Geophys. J. Int. (2004) **159,** 711–720 doi: 10.1111/j.1365-246X.2004.02432.x

Shear wave splitting in three-dimensional anisotropic media

Sébastien Chevrot,[1] Noémie Favier[1] and Dimitri Komatitsch[2]

[1] *Laboratoire de Dynamique Terrestre et Planétaire, CNRS, UMR* 5562, *Observatoire Midi-Pyrénées, Université Paul Sabatier, Toulouse, France*
[2] *Laboratoire d'Imagerie Géophysique, CNRS, FRE* 2639, *Université de Pau et des Pays de l'Adour, Pau, France*

Accepted 2004 July 29. Received 2004 April 16; in original form 2003 August 25

SUMMARY

Splitting intensity, a new seismic observable that characterizes seismic anisotropy, can be expressed as linear combinations of elastic perturbations involving 3-D sensitivity (or Fréchet) kernels. We conduct a numerical study of elastic wave propagation in weakly anisotropic heterogeneous media in order to investigate the validity of the different assumptions made in the derivation of these kernels. For characteristic periods larger than 6 s, the splitting parameters obtained from the analysis of synthetic seismograms calculated using a spectral-element method (SEM) are in excellent agreement with predictions based upon the 3-D kernels. This suggests that the kernels fully capture the complexity of shear wave splitting in heterogeneous anisotropic media and can be used for tomography. In addition, they can be used to calculate synthetic splitting parameters in 3-D anisotropic media, which represents a very small amount of computation compared with finite-difference or finite-element modelling. 3-D kernels distribute sensitivity off of the reference ray given by the laws of geometrical optics. This has important consequences for the interpretation of apparent splitting parameters, which usually relies on ray theory. Apparent splitting parameters estimated at the surface can differ significantly from the anisotropic properties in the underlying medium wherever heterogeneities occur with a characteristic wavelength smaller than approximately 0.75 times the width of the first Fresnel zone $\sqrt{\lambda z}$, with λ the wavelength and z the depth.

Key words: anisotropy, Fréchet kernels, shear wave splitting.

1 INTRODUCTION

By far the most frequently used method to study seismic anisotropy of the upper mantle is the analysis of *SKS* splitting, introduced by Vinnik *et al.* (1984). This approach has many advantages. First, conversions at the core–mantle boundary suppress any splitting that could have been acquired by the wave in the source region. Secondly, *SKS* waves are radially polarized and a detectable signal on the transverse component is probably the least ambiguous manifestation of seismic anisotropy observed on seismograms. The popularity of this method also comes from its simplicity and from the common belief that, in spite of their lack of vertical resolution, *SKS* waves provide excellent lateral resolution owing to their subvertical incidence. It is therefore often assumed that, in contrast to surface waves, *SKS* waves can resolve spatial variations of anisotropy over short distances. Based on this assumption, shear wave splitting measurements are almost invariably interpreted in terms of anisotropy orientation and magnitude in the underlying medium.

This point of view implicitly relies on geometrical optics, or ray theory, and assumes that spatial variations of anisotropy are smooth over a wavelength. However, owing to their dominant period around 10 s, shear waves are sensitive to a broad region around the ray path. Alsina & Snieder (1995) gave the first qualitative estimates of the size of *SKS* Fresnel zones. Using a Kirchhoff integration, they modelled vertically propagating shear waves in a medium composed of two adjacent blocks with different anisotropic properties. The analysis of the synthetic seismograms showed a transition region where the anisotropic properties result from a complex spatial average over the two blocks. They estimated the size of the Fresnel zone from the width of the transition region where these complex signatures were observed. Considering *SKS* waves recorded by close stations, simple arguments based on the width of the Fresnel zone led them to put some constraints on the depth distribution of anisotropy. Rümpker & Ryberg (2000) later conducted a similar estimate of the size of the Fresnel zone based on finite-difference synthetic seismograms and obtained comparable results.

More recently, Favier & Chevrot (2003) have shown that a new seismic observable, called splitting intensity, is to first order linearly related to the elastic perturbations of the medium through 3-D sensitivity (or Fréchet) kernels. This new formalism allows to compute the 3-D sensitivity kernels directly, which constitutes a clear improvement over previous studies that gave only indirect estimates of the size of the Fresnel zone. In addition, the kernels allow the formulation of a linear tomographic problem, which opens new perspectives for high-resolution imaging of upper-mantle anisotropy. Although it is now possible to simulate wave propagation in the global 3-D earth (Komatitsch & Tromp 2002), the cost of these simulations is still too prohibitive to use them for inversion, at least

for short-period body waves. However, such 3-D simulations can be used to explore the limits of validity of the various assumptions that are commonly made in regional and global tomographic studies and to quantify the improved description of wave propagation offered by sensitivity kernels compared with ray theory. Hung *et al.* (2000) presented the first numerical investigations of this kind for the case of 3-D wave propagation in acoustic media. In this article, we follow a similar approach to extend their results to the case of shear wave propagation in transversely isotropic (or hexagonal) media.

In Section 2, we present a simplified description of shear wave splitting. We then describe briefly in Section 3 the theory of 3-D Fréchet kernels for splitting intensity. In Section 4, we conduct a numerical study of the validity of the 3-D kernels. We use a spectral-element method (SEM) for the numerical simulation of wave propagation in 3-D heterogeneous anisotropic media and compare the splitting parameters measured on the synthetic seismograms with those predicted by the 3-D kernels. Another comparison with the predictions of ray theory allows us to define precisely its limits of validity. In the final section, we show that our numerical study has several important consequences for the interpretation of shear wave splitting measurements and for the imaging of anisotropy.

2 GEOMETRICAL RAY THEORY

We first present the point of view of geometrical optics that supports the analysis of *SKS* splitting. Let us consider the simple case of a plane shear wave propagating vertically in a homogeneous transversely isotropic medium with a horizontal axis of symmetry. If $w(t)$ is the wavelet shape of the incoming wave, δt the delay time between the two quasi-shear waves and β the angle between the symmetry axis and the direction of polarization of the incident wave, the signals on the radial and transverse components are given by (e.g. Silver & Chan 1991):

$$u_{\mathrm{R}}(t) = \cos^2\beta w(t+\delta t/2) + \sin^2\beta w(t-\delta t/2), \tag{1}$$

$$u_{\mathrm{T}}(t) = -\frac{1}{2}\sin 2\beta\,[w(t+\delta t/2) - w(t-\delta t/2)]\,. \tag{2}$$

For a small delay time δt compared with the dominant period of the signal, these expressions can be further simplified:

$$u_{\mathrm{R}}(t) = w(t), \tag{3}$$

$$u_{\mathrm{T}}(t) = -\frac{1}{2}\delta t \sin 2\beta w'(t), \tag{4}$$

where $w'(t)$ denotes the time derivative of $w(t)$. Therefore, the transverse component is simply the time derivative of the radial component multiplied by a factor that is defined as the splitting intensity S. Splitting intensity is easily obtained from seismological records by projecting the transverse component on the derivative of the radial component (Chevrot 2000):

$$S = -2\frac{\int_{-\infty}^{+\infty} -i\omega u_{\mathrm{T}}(\omega) u_{\mathrm{R}}^{0*}(\omega)\,d\omega}{\int_{-\infty}^{+\infty} \omega^2 \left|u_{\mathrm{R}}^{0*}(\omega)\right|^2 d\omega}. \tag{5}$$

Studying the variations of S as a function of ϕ, the polarization of the incoming wave, is a powerful technique to determine the splitting parameters δt, the delay time, and ϕ_0, the orientation of the symmetry axis. Depth-dependent anisotropy produces a splitting intensity that represents the vertical integration of splitting intensities over all the anisotropic layers crossed by the seismic wave.

In the particular case of a homogeneous weakly anisotropic medium, if the scale of lateral variations is much larger than the wavelength (i.e. if geometrical optics is valid), splitting intensity is simply:

$$S = \delta t \sin 2(\phi - \phi_0), \tag{6}$$

i.e. it has a sinusoidal variation with backazimuth.

3 3-D SENSITIVITY KERNELS

In a spherical isotropic earth model, the transverse component of *SKS* waves is zero. Anisotropic perturbations of this reference isotropic medium generate a signal on the transverse component that can be seen as a perturbation of displacement. Using first-order perturbation theory (i.e. Born approximation) it is straightforward to calculate the perturbation of the transverse component of the displacement produced by anisotropic elastic perturbations of the reference medium (e.g. Gibson & Ben-Menahem 1991; Chapman & Coates 1994). For the case of transversely isotropic perturbations and a symmetry axis lying in the horizontal plane, the perturbed displacement is given by (Favier & Chevrot 2003):

$$\delta u_{\mathrm{T}}(\mathbf{r_0}, t) = \int_V \frac{\omega^2}{4\pi\beta^2 r}\gamma(\mathbf{r}) F(\theta,\phi,\alpha,\phi_0) e^{-i\omega r/\beta} u_{\mathrm{R}}^0(\mathbf{r}, t)\,d^3\mathbf{r}, \tag{7}$$

where $\gamma = (C_{66} - C_{44})/2C_{44}$ is the anisotropic parameter defined by Mensch & Rasolofosaon (1997) and β is the shear wave velocity in the reference medium. The function $F(\theta,\phi,\alpha,\phi_0)$ represents the radiation pattern for a transversely isotropic elastic perturbation:

$$F(\theta,\phi,\alpha,\phi_0) = \sin\theta[\cos^2\theta\sin 2(\phi-\phi_0) + \sin^2\theta\sin 2(\alpha-\phi_0)], \tag{8}$$

where θ is the angle between the direction of wave propagation and the horizontal plane, ϕ the scattered wave azimuth, α the polarization of the incoming shear wave and ϕ_0 the azimuth of the symmetry axis (Fig. 1). The generalization of eq. (7) to cases corresponding to a lower order of symmetry is straightforward. However, considering lower symmetry classes requires a larger number of elastic parameters that would be difficult to constrain from seismic observations alone.

Using eq. (7) in eq. (5) we can write the splitting intensity as a volumetric integral of the anisotropic perturbations multiplied by two anisotropic kernels K_C and K_S that correspond to the Fréchet derivatives of splitting intensity with respect to the elastic perturbations $\gamma_C = \gamma\cos 2\phi_0$ and $\gamma_S = \gamma\sin 2\phi_0$, respectively:

$$S = \int_V \gamma_C(\mathbf{r}) K_C(\mathbf{r_0}, \mathbf{r}; \alpha)\,d^3\mathbf{r} + \int_V \gamma_S(\mathbf{r}) K_S(\mathbf{r_0}, \mathbf{r}; \alpha)\,d^3\mathbf{r}, \tag{9}$$

with the Fréchet derivatives given by (Favier & Chevrot 2003)

$$K_C(\mathbf{r_0}, \mathbf{r}; \alpha) = \frac{1}{4\pi\beta^2 r}\sin\theta(\cos^2\theta\sin 2\phi + \sin^2\theta\sin 2\alpha)\frac{\int_{-\infty}^{+\infty}\omega^3|u_{\mathrm{R}}(\omega)|^2\sin(\omega\Delta t)\,d\omega}{\int_{-\infty}^{+\infty}\omega^2|u_{\mathrm{R}}(\omega)|^2\,d\omega}, \tag{10}$$

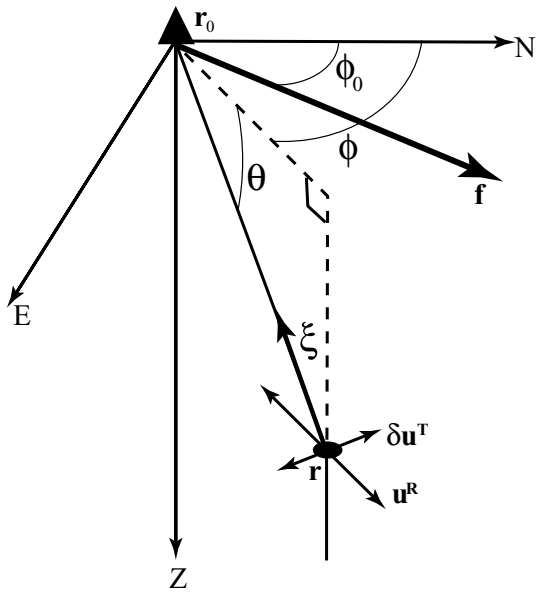

Figure 1. Notations used to describe scattering. The axis **f** represents the fast symmetry axis. The scattering point is located at **r**. The unit vector $\boldsymbol{\zeta}$ pointing from **r** towards $\mathbf{r_0}$, the position of the receiver, is described by its azimuth ϕ and elevation θ.

$$K_S(\mathbf{r_0}, \mathbf{r}; \alpha) = \frac{-1}{4\pi\beta^2 r} \sin\theta(\cos^2\theta \cos 2\phi + \sin^2\theta \cos 2\alpha) \frac{\int_{-\infty}^{+\infty} \omega^3 |u_R(\omega)|^2 \sin(\omega \Delta t)\, d\omega}{\int_{-\infty}^{+\infty} \omega^2 |u_R(\omega)|^2\, d\omega}, \tag{11}$$

where Δt is the time difference between reference and scattered rays (Favier & Chevrot 2003). Eq. (9) can be seen as a generalization of eq. (6) when small-scale variations (i.e. variations at scales smaller than the size of the Fresnel zone) are present and for finite-frequency waves.

4 NUMERICAL MODELLING

Our main goal in this section is to investigate the validity of eqs (6) and (9) by comparing their predictions with the results obtained by numerical modelling of full wave propagation in 3-D anisotropic media.

4.1 Description of the method

We compute synthetic seismograms based upon the SEM, which is a highly accurate technique to model seismic wave propagation in elastic or anelastic media (e.g. Komatitsch & Tromp 2002). While most classical numerical techniques used in seismology, such as the finite-difference method (FDM) (Virieux 1986), are based upon the differential (or strong) form of the seismic wave equation, the SEM is based upon the variational (or weak) form, which is obtained by dotting it with a so-called test vector and integrating by parts over the region under study. The SEM can take into account the full anisotropic elastic tensor with 21 coefficients (Komatitsch *et al.* 2000). It is more precise than the FDM in this context because even for a full anisotropic tensor no interpolation of material properties or field components is needed (Komatitsch *et al.* 2000). The SEM is also computationally more efficient than classical finite-element techniques (e.g. Bao *et al.* 1998) because the mass matrix is exactly diagonal by construction (e.g. Komatitsch & Tromp 1999), which implies that no linear system of equations needs to be inverted and that as a result fully explicit time schemes can be used.

We simulate the propagation of a plane wave, which is introduced in the explicit time marching scheme as an initial Gaussian-shape analytical displacement and its corresponding velocity field. On the edges of the grid, following the ideas of Bielak & Christiano (1984), we subtract at each time step the contour integral of the traction produced by the analytical source, whose expression appears in the integration by parts used to obtain the variational formulation of the wave equation.

4.2 Validity of 3-D sensitivity kernels

For a homogeneous anisotropic layer, the splitting intensity is given by eq. (6) if the delay time is small compared with the dominant period of the signal (or equivalently if anisotropy is weak). The 3-D sensitivity kernels also predict a sinusoidal splitting intensity as a function of backazimuth (Favier & Chevrot 2003). We design a first numerical experiment to investigate the domain of validity of the small delay time (or weak anisotropy) assumption.

We consider a volume that is meshed using cubes with a volume of $12.5 \times 12.5 \times 8$ km^3. We use polynomials of degree $N = 4$ in each direction of each spectral element to discretize the wavefield. The total number of spectral elements in the mesh is $64 \times 64 \times 50 = 204\,800$, which corresponds to a total of approximately 13 000 000 independent grid points. The time step is 75 ms and we simulate a total duration of 90 s of propagation. Using this mesh and a shear wave velocity of 5 km s^{-1} for the isotropic reference medium, we can calculate synthetic seismograms that are accurate down to a period of ∼3 s. The number of grid points per minimum wavelength is ∼5. We simulate shear waves that propagate vertically through an anisotropic layer located between 32 and 160 km depth with a fast axis oriented at $\phi_0 = 0^\circ$ (Fig. 2). We vary the dominant period of the incident plane wave between 3 and 14 s for three

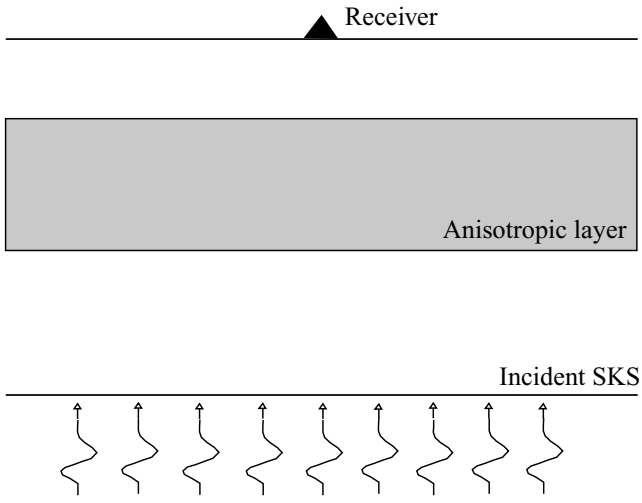

Figure 2. Model configuration used for the numerical simulation of 3-D wave propagation. The grey region represents the anisotropic layer embedded in a homogeneous isotropic medium. A receiver located at the free surface records a plane shear wave that propagates vertically.

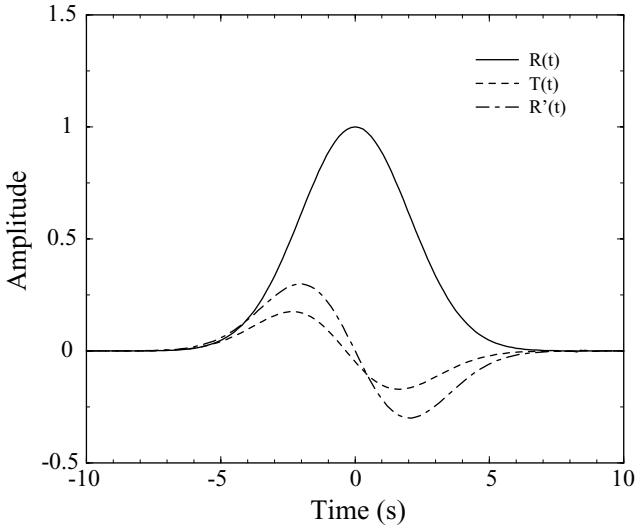

Figure 3. Radial and transverse components of the synthetic seismogram for the model configuration shown in Fig. 2. The anisotropic layer is located between 32 and 160 km depth and has 5 per cent anisotropy, which corresponds to a delay $\delta t = 1.28$ s and a fast axis oriented at $\phi_0 = 0^\circ$. The dominant period of the plane wave is 12.7 s. The derivative of the radial component is also shown for comparison and is approximately proportional to the transverse component.

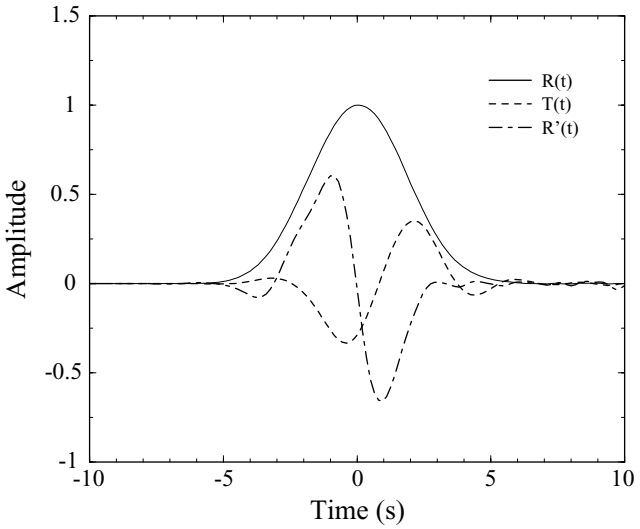

Figure 5. Radial and transverse components of the synthetic seismogram for the model configuration shown in Fig. 2. The anisotropic layer is located between 32 and 160 km depth and has 15 per cent anisotropy, which corresponds to a delay $\delta t = 1.92$ s and a fast axis oriented at $\phi_0 = 0^\circ$. The dominant period of the plane wave is 5.7 s. The derivative of the radial component is also shown for comparison and is clearly not proportional to the transverse component.

different levels of anisotropy: 5 per cent ($\delta t = 1.28$ s), 7.5 per cent ($\delta t = 1.92$ s) and 15 per cent ($\delta t = 2.56$ s). In addition, in a last set of simulations, we use a thinner anisotropic layer located between 32 and 96 km depth with 5 per cent anisotropy, which corresponds to a delay $\delta t = 0.64$ s.

Fig. 3 shows the radial and transverse components as well as the derivative of the radial component of the synthetic seismogram corresponding to a delay time $\delta t = 1.28$ s and a dominant period of 12.7 s. The transverse component is approximately proportional to the derivative of the radial component, which is in agreement with eq. (4). Splitting intensity, measured by projecting the transverse component onto the derivative of the radial component according to eq. (5), is shown in Fig. 4 for different polarizations of the incoming wave. Splitting intensity as a function of backazimuth is a sinusoid. From its amplitude we can deduce the delay time δt and from its phase the azimuth ϕ_0 of the symmetry axis.

Fig. 5 shows the components of the synthetic seismogram corresponding to a delay time $\delta t = 1.96$ s and a dominant period of 5.7 s. In contrast to the previous case, the transverse component is no longer proportional to the derivative of the radial component. Splitting intensity as a function of backazimuth, shown in Fig. 6, while still periodic, is no longer a sinusoid. The solid line shows the sinusoid that best fits the measured splitting intensity. The amplitude of this sinusoid is much smaller than the maximum splitting intensity, which suggests that the approximate expressions given by eqs (3), (4) and (6) are no longer valid.

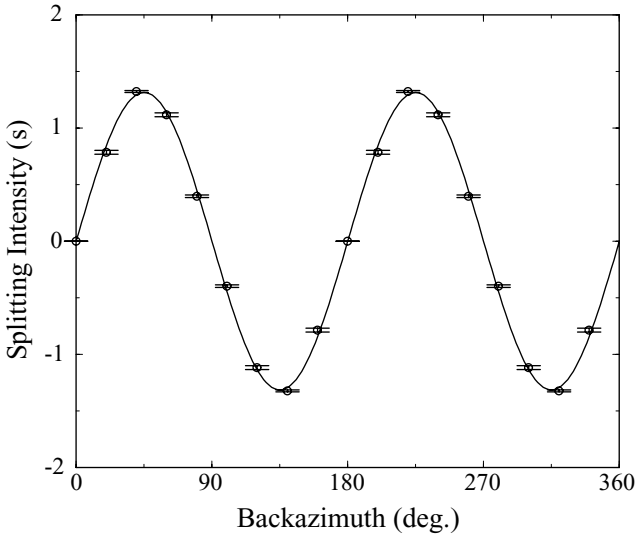

Figure 4. Splitting intensity as a function of backazimuth (solid circle) and the sinusoid that best fits these measurements (solid line) for the model described in Fig. 3.

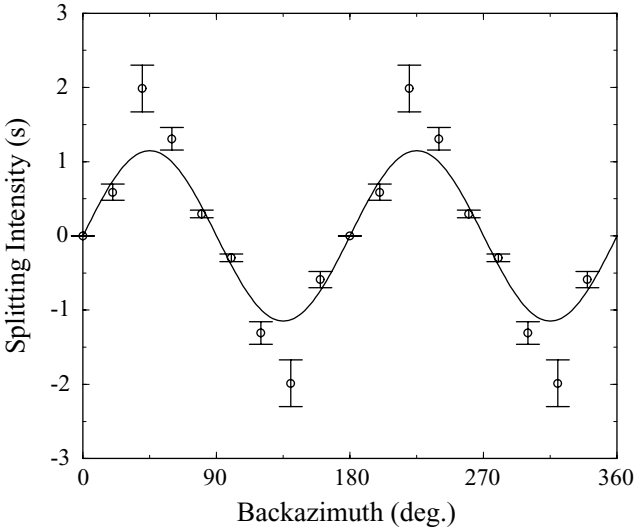

Figure 6. Splitting intensity as a function of backazimuth (solid circle) and the sinusoid that best fits these measurements (solid line) for the model described in Fig. 5.

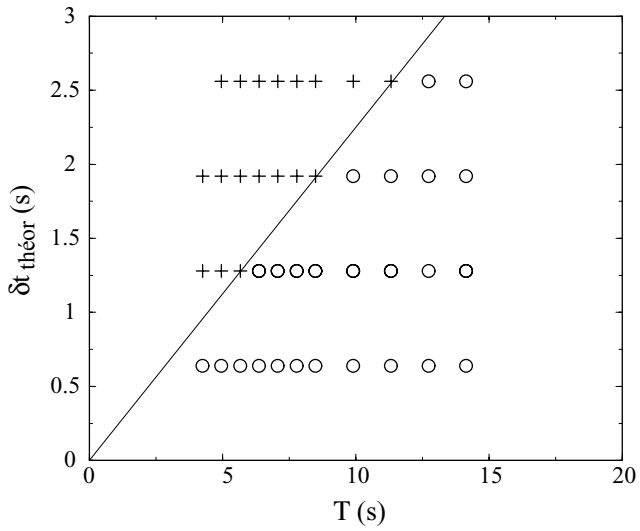

Figure 7. Diagram summarizing the results of the numerical experiments performed using the model configuration shown in Fig. 2 and different dominant periods T of the signal. For each experiment, we determine the delay time by fitting a sinusoid to the splitting intensity measurements. The circles show the experiments for which the measured delay time differs by less than 5 per cent from the theoretical delay time. The crosses show the experiments for which the difference is larger than 5 per cent. The results define a domain of validity that is located approximately below the line $\delta t = \sqrt{2}/2\pi T \approx 0.225T$.

The results of all the numerical experiments are summarized in Fig. 7. The circles represent the experiments for which the measured delay time, obtained by fitting a sinusoid to the variations of splitting intensity with backazimuth, deviate from the theoretical delay time by less than 5 per cent, which is a typical error level in real measurements (Chevrot 2000). The crosses represent the experiments for which the differences are larger than 5 per cent. These results allow us to define two domains in the (δt, T) space that are separated by the line $\delta t = \sqrt{2}/2\pi T \approx 0.225T$, where T is the dominant period of the signal. In the lower domain, the approximate expressions given by eqs (3), (4) and (6) are valid and consequently the 3-D kernels provide an accurate description of shear wave splitting.

Petrofabrics analysis of peridotite nodules has shown that shear wave anisotropy should be around 5 per cent at temperature and pressure conditions found in the top 200 km of the mantle (Mainprice & Silver 1993; Mainprice *et al.* 2000). For this level of anisotropy and a thickness of the anisotropic layer of 128 km, our results show that measurements can be performed at a dominant period as low as approximately 6 s. 3-D kernels can be used to compute splitting parameters inside their domain of validity, which is particularly interesting because their calculation is computationally far less expensive than 3-D SEM numerical modelling.

4.3 Validity of ray theory

In order to determine the validity of geometrical ray theory to describe shear wave splitting, we consider the propagation of a finite-frequency plane wave through a single homogeneous spherical anisotropic inclusion, as illustrated in Fig. 8. In all the simulations anisotropy inside the inclusion is 3 per cent and the dominant wavelength is 50 km. We determine the shear wave splitting parameters at a receiver located at the surface, right above the anisotropic inclusion. Following Baig *et al.* (2003), we introduce the doughnut-hole

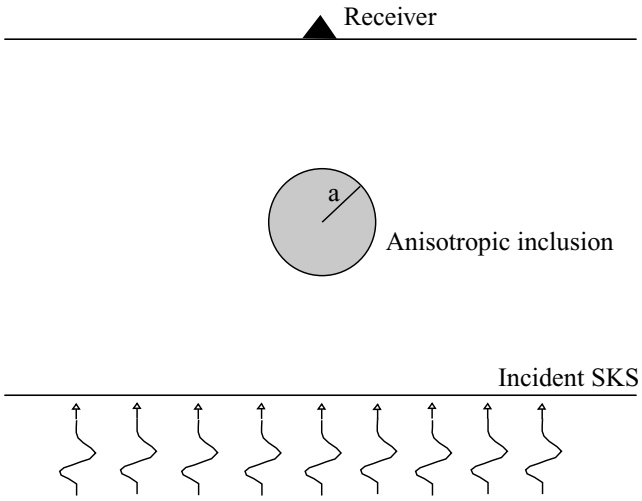

Figure 8. Model configuration used in the numerical simulation of 3-D wave propagation. The grey region represents an anisotropic sphere of radius a embedded in a homogeneous isotropic medium. A receiver located at the free surface records a shear wave that propagates vertically.

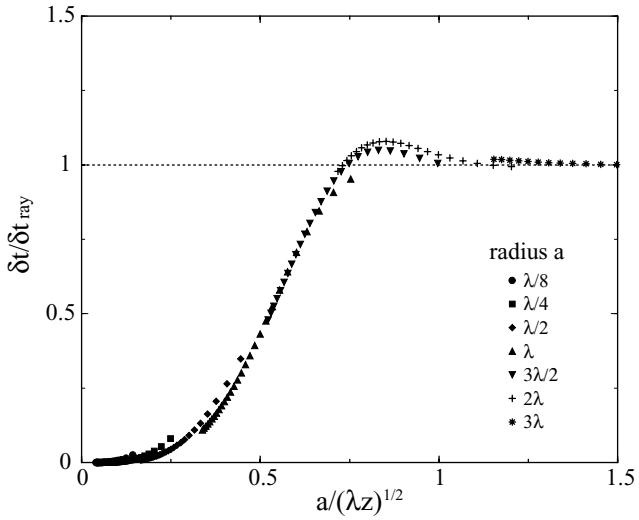

Figure 9. Diagram summarizing the results of the different numerical experiments using the model configuration shown in Fig. 8 and an anisotropic spherical region with radius a at varying depth. For each experiment we determine the delay time by fitting a sinusoid to the splitting intensity measurements.

parameter, defined as the dimensionless ratio between the radius a of the anisotropic inclusion and the width of the Fresnel zone, $\sqrt{\lambda z}$.

Fig. 9 shows the ratio between the true delay time and the delay time given by ray theory versus the doughnut-hole parameter. The different branches correspond to a fixed radius a, which varies between $\lambda/8$ and 3λ. We vary the position of the inclusion between 30 and 400 km depth, with 10 km depth increments. All the measurements are represented on the same plot and clearly fall on the same curve, which allows us to define the validity of ray theory as a function of the scale of the heterogeneities. Three different regimes can be identified. For length scales larger than the width of the Fresnel zone, the ratio between the true delay time and the ray theory delay time is close to unity and ray theory is uniformly valid. For doughnut-hole parameters between 0.75 and 1, the ratio is slighty larger than unity, an effect that comes from subtracting part

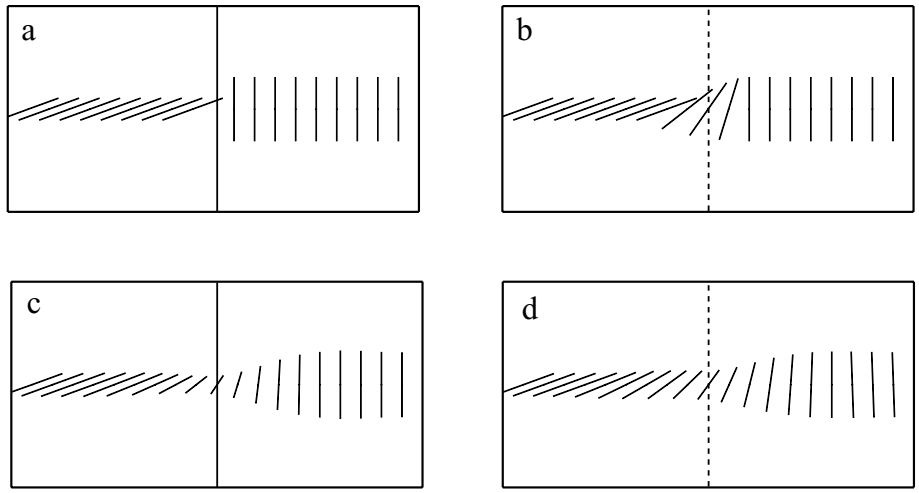

Figure 10. (a) Map view of anisotropy inside the two-block model. (b) Map view of anisotropy inside the transition model. (c) Apparent splitting parameters measured at the surface for model (a). (d) Apparent splitting parameters measured at the surface for model (b).

of the contribution of the second Fresnel zone. For doughnut-hole parameters smaller than 0.75, the ratio decreases when the normalized length scale decreases. As expected, very small inclusions can fit into the hole of the kernels, and delay time tends to zero. From Fig. 9, we therefore conclude that the critical value for the radius of the inclusion is approximately $0.75\sqrt{\lambda z}$.

For a wavelength of 40 km, a typical value for *SKS* phases, and a depth of 100 km, the critical diameter of the inclusion is approximately 95 km. This means that if anisotropy varies significantly over distances smaller than 100 km, geometrical ray theory is no longer valid and the apparent anisotropic properties derived from surface observations are no longer simply related to the anisotropy in the underlying medium. Numerous global studies have documented variations of shear wave splitting over short distances (typically a few degrees) on continents (e.g. Helffrich *et al.* 1994; Silver 1996). However, only regional-scale studies are able to resolve variations over distances smaller than 100 km. Indeed, it is the observation of strong variations of apparent splitting parameters under the Netherlands and Belgium that first led Alsina & Snieder (1995) to investigate the 3-D sensitivity of *SKS* phases to anisotropy. More recently, using a dense network of permanent and mobile stations, Babuška *et al.* (2002) observed strong variations of splitting parameters over distances smaller than 50 km, allowing them to distinguish three lithospheric domains in the French Massif Central with different seismic anisotropy. Fouch *et al.* (2004) also observed strong variations of delay times with a small aperture (∼40 km) array near Kimberley, in South Africa. Therefore, observations of shear wave splitting in continents suggest that short-scale variations in anisotropy are indeed present and that 3-D effects cannot be neglected.

5 IMPLICATIONS FOR THE INTERPRETATION OF SHEAR WAVE SPLITTING MEASUREMENTS

5.1 Sharp versus smooth variations of anisotropy

Continents juxtapose lithospheric blocks accreted during their long and complex tectonic history. If the anisotropy were a manifestation of a frozen lithospheric fabric, we could expect sharp contrasts across the sutures separating lithospheric blocks. Similarly, a narrow shear zone resulting from the localization of lithospheric deformation would presumably generate a strong contrast in anisotropy with the surrounding lithosphere. Can seismic observations collected at the surface detect such sharp transitions? Answering this question is not easy because, as we have seen in previous sections, long-period shear waves sample the anisotropic properties of the Earth in a complex fashion.

A suture between two lithospheric blocks with different fabrics can be modelled by two simple blocks (see Fig. 10a). The anisotropic layer between 32 and 160 km depth has 3 per cent anisotropy. For the sake of simplicity, we first consider plane *S* waves propagating vertically with a dominant period of 10 s. Fig. 11 shows splitting intensity as a function of backazimuth obtained by analysing the SEM synthetic seismograms and by integrating the 3-D kernels for the receiver located above the two blocks. The agreement between the two approaches is remarkable, which was expected because the case considered is in the domain of validity of the small delay assumption (see previous section). The other stations (not shown here)

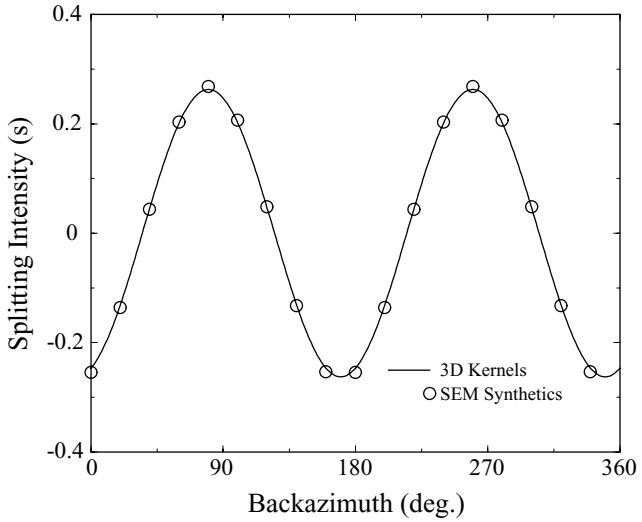

Figure 11. Splitting intensity as a function of backazimuth for the receiver located above the boundary between the two blocks in the geometry shown in Fig. 10(a) obtained from the analysis of the SEM synthetic seismograms (circles) and from the integration of 3-D kernels (solid line).

show a similar level of consistency between SEM modelling and 3-D kernels. The apparent splitting parameters for all the stations obtained from the analysis of the SEM synthetic seismograms appear in Fig. 10(c). Most striking is the apparent continuous rotation of the fast direction from $\phi = 70^\circ$ in the left block to $\phi = 0^\circ$ in the right block. The sharp transition of anisotropy at depth produces a smooth variation of the apparent splitting parameters at the surface over a range of approximately 40 km. This remarkable feature can be explained by the sensitivity of finite-frequency shear waves to anisotropy off the geometrical ray path (Favier & Chevrot 2003). The apparent splitting parameters reflect the true level of anisotropy that is located directly in the underlying medium only far from the boundary between the two blocks.

To investigate the possibility of distinguishing sharp and smooth transitions, we perform a second numerical experiment in which the anisotropic properties vary smoothly from one block to the other (Fig. 10b). The width of the gradient zone is 20 km, the apparent width of the transition observed in the first experiment. If the anisotropy were deeper or the dominant period larger, the width of the transition zone would be larger. Apparent splitting parameters measured at the surface appear in Fig. 10(d). The apparent fast axis directions are very similar to those obtained in the first experiment. However, the apparent delay times are smaller for the sharp transition case than for the smooth transition case. Therefore, discriminating between the two models requires both a robust measurement technique that remains accurate at small delay times (e.g. Chevrot 2000) and a good sampling of the wavefield near the boundaries.

5.2 Isotropy, vertical symmetry axis or boundary between two anisotropic domains

Delay times smaller than 0.5 s are difficult to measure using classical data analysis techniques and are usually considered as null measurements (e.g. Silver & Chan 1991). These null measurements are often interpreted as the presence of an anisotropic layer too thin to be detected, or of an anisotropic layer with a subvertical symmetry axis. Our results suggest another possibility: small-scale lithospheric heterogeneity. A receiver located in a region where anisotropy varies rapidly over short distances in orientation (but not necessarily in amplitude) will record a much smaller splitting than a receiver located in a homogeneous region. Discriminating between these three hypotheses requires resolving small-scale lateral variations and stratification of anisotropy, which is impossible from a single-station analysis or if stations are separated by a distance larger than the width of the first Fresnel zone. Whether continental lithosphere is composed of blocks with well-developed fabrics thus remains an interesting question open for future studies involving dense arrays of broad-band stations.

5.3 Lateral versus vertical variations of anisotropy

Numerical simulations of wave propagation in depth-dependent anisotropic media have shown that apparent splitting parameters are frequency-dependent (Rümpker *et al.* 1999; Saltzer *et al.* 2000). In addition, the apparent fast direction is weighted towards the orientation in the shallower part of the mantle (Saltzer *et al.* 2000). In contrast, Favier *et al.* (2004) have shown that at long periods (i.e. periods in the lower domain in Fig. 7), sensitivity to anisotropy is constant with depth. Because different measurement techniques were used, these results are not necessarily contradictory. The former studies used the technique of Silver & Chan (1991), which consists of finding the combination of delay time and fast direction that minimizes the energy on the transverse component after correction for shear wave splitting. The latter study measured the delay time and fast direction from observed variations of splitting intensity as a function of the backazimuth of the incoming wave (Chevrot 2000). This difference in measurement techniques may also explain why, in spite of the fact that they used the same two-block model, Favier & Chevrot (2003) were able to determine splitting parameters in the boundary region while Rümpker & Ryberg (2000) found them less reliable and considered them as null measurements. A brief comparison between the two measurement techniques is presented in the Appendix. In any case, splitting intensity, in contrast to fast polarization direction, is a seismic observable that is linearly related to perturbations of the elastic parameters. Therefore, we believe that it is simpler to study anisotropy based upon this new seismic observable, and that this opens new and important perspectives in the context of 3-D anisotropic tomography.

Because the size of the Fresnel zone depends on the dominant period of the waves, if anisotropy varies over distances smaller than the width of the first Fresnel zone, the apparent splitting parameters will depend on period. To illustrate this effect, we consider the same two-block model as in Fig. 10(a). In a broad region above the boundary, apparent splitting parameters display significant variations when the period varies between 8 and 16 s (Figs 12 and 13). For example, a receiver located 20 km east of the boundary exhibits variations of 0.2 s for the delay time and 5° for the fast polarization direction, which is significant. Because the width of the Fresnel zone increases with depth, apparent splitting parameters are sensitive to both lateral and vertical variations of anisotropy, though the former are expected to dominate. This property can be exploited by measuring splitting parameters at different frequencies in order to improve spatial resolution. For example, this would help to discriminate between the sharp and smooth transition models because the differences in their anisotropic signature would be more pronounced at other frequencies. In any case, separating lateral and vertical variations of anisotropy requires a good sampling of the medium, which can only be obtained by using a dense array of broad-band stations.

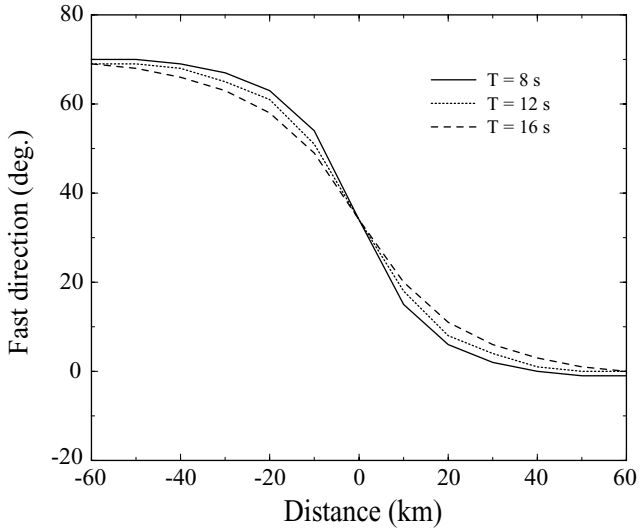

Figure 12. Apparent fast direction measured at the surface for the model shown in Fig. 10(a) for plane waves with a dominant period of 8, 12 and 16 s, respectively, as a function of the distance from the boundary between the two blocks.

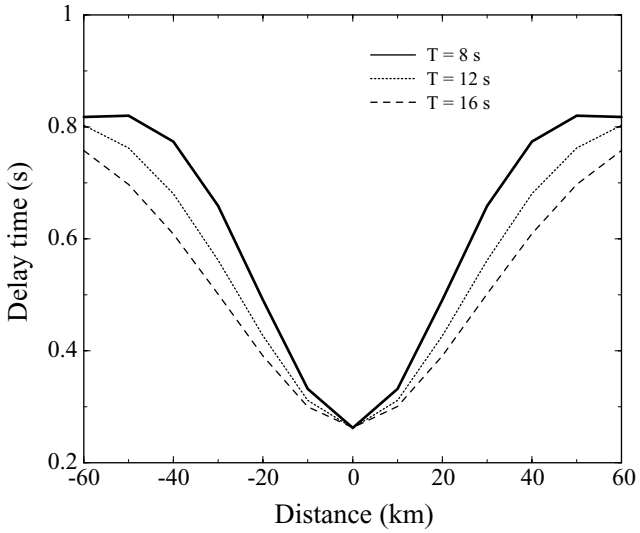

Figure 13. Apparent delay times measured at the surface for the model shown in Fig. 10(a) for plane waves with a dominant period of 8, 12 and 16 s, respectively, as a function of the distance from the boundary between the two blocks.

5.4 Apparent variations of splitting parameters with backazimuth

Fig. 11 shows splitting intensity measured at the receiver located above the boundary between the two blocks for the geometry shown in Fig. 10(a). For a plane *SKS* wave propagating vertically, variations of splitting intensity as a function of backazimuth are very well described by a sinusoid even though lateral and vertical heterogeneities are present.

On the other hand, the 3-D sensitivity kernels for a 10° incidence angle, a typical incidence angle of *SKS* waves, are no longer symmetric with respect to the vertical axis (Fig. 14). The break of symmetry is mainly a result of the complex dependence of the radiation pattern of a transversely isotropic elastic perturbation on the angle between the propagation direction of the scattered wave and the symmetry axis (see fig. 2 in Favier & Chevrot 2003). Fig. 15 shows splitting intensity at the station located above the boundary between the two blocks as a function of backazimuth for a constant 10° incidence angle. In the case of oblique incidence, the 180° periodicity of splitting intensity is broken. Shear wave splitting is no longer described by unique splitting parameters δt and ϕ_0, and these parameters present apparent variations with backazimuth. Even more surprising, waves coming from the same backazimuth but with different incidence angles (depending on the epicentral distance) can show significant differences in shear wave splitting. However, the sinusoidal fit to the splitting intensity data still provides average splitting parameters that can be seen as analogous to station residuals that represent the average traveltime perturbation seen by a seismic station. Deviations from the optimal sinusoid give splitting intensity residuals that can be used to map 3-D lithospheric and asthenospheric anisotropic structures.

This last result should have important consequences on the studies of apparent variations of splitting parameters with backazimuth that are often interpreted as indications of stratification of anisotropy (e.g. Savage & Silver 1993). Our numerical experiments demonstrate that complex and counter-intuitive 3-D propagation effects are important and should be taken into account. These effects would be even stronger and more complicated if the dip of the symmetry axis were allowed to vary in any direction and were not constrained to be in the horizontal plane, as in the present study.

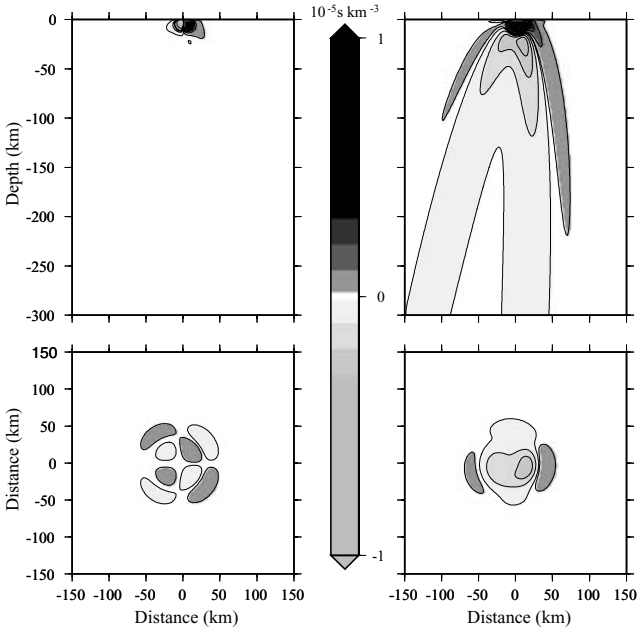

Figure 14. Splitting intensity sensitivity kernels K_C (left) and K_S (right) for a 10° incidence angle and an incident wave polarized in the N–S direction. The top diagrams show the N–S cross-sections. The bottom diagrams show horizontal cross-sections at 40 km depth. Note that the kernels are no longer symmetric with respect to the vertical axis.

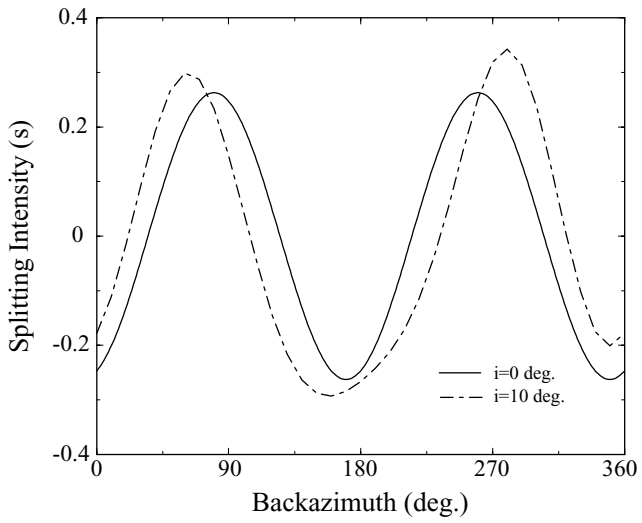

Figure 15. Splitting intensity as a function of backazimuth for the receiver located above the boundary between the two blocks in the geometry shown in Fig. 10(a) for a vertical incidence and for an incidence angle of 10°.

6 CONCLUSIONS

We have shown that the apparent fast direction observed at the surface can deviate significantly from the symmetry axis orientation in the underlying medium in regions where lateral variations with a characteristic wavelength smaller than the size of the Fresnel zone (typically around 100 km for a shear wave with a dominant period of 10 s) are present. Fréchet kernel theory accounts for this

finite-frequency effect that smears the sensitivity to anisotropy away from the geometrical ray path.

Anisotropy beneath oceanic lithosphere is likely coherent over regions comparable in size to plates. In contrast, there is increasing evidence for the presence of strong variations of apparent splitting parameters over short distances under continents (e.g. Helffrich *et al.* 1994; Alsina & Snieder 1995; Silver 1996; Babuška *et al.* 2002; Fouch *et al.* 2004). Thus, in order to constrain unambiguously seismic anisotropy under continents, seismologists will have to use dense arrays of broad-band stations and account for finite-frequency effects on shear wave splitting.

ACKNOWLEDGMENTS

This work was supported in part by the INSU programme 'Intérieur de la Terre'.

REFERENCES

Alsina, D. & Snieder, R., 1995. Small-scale sublithospheric continental mantle deformation: constraints from SKS splitting observations, *Geophys. J. Int.,* **123,** 431–448.

Babuška, V., Plomerová, J., Vecsey, L., Granet, M. & Achauer, U., 2002. Seismic anisotropy of the French Massif Central and predisposition of Cenozoic rifting and volcanism by Variscan suture hidden in the mantle lithosphere, *Tectonics,* **21,** 10129/2001TC901035.

Baig, A.M., Dahlen, F.A. & Hung, S.H., 2003. Traveltimes of waves in three-dimensional random media, *Geophys. J. Int.,* **153,** 467–482.

Bao, H., Bielak, J., Ghattas, O., Kallivokas, L.F., O'Hallaron, D.R., Shewchuk, J.R. & Xu, J., 1998. Large-scale simulation of elastic wave propagation in heterogeneous media on parallel computers, *Comput. Methods Appl. Mech. Eng.,* **152,** 85–102.

Bielak, J. & Christiano, P., 1984. On the effective seismic input for nonlinear soil-structure interaction systems, *Earthquake Eng. Struct. Dyn.,* **12,** 107–119.

Chapman, C.H. & Coates, R.T., 1994. Generalized Born scattering in anisotropic media, *Wave Motion,* **19,** 309–341.

Chevrot, S., 2000. Multichannel analysis of shear wave splitting, *J. Geophys. Res.,* **105,** 21 579–21 590.

Favier, N. & Chevrot, S., 2003. Sensitivity kernels for shear wave splitting in transverse isotropic media, *Geophys. J. Int.,* **153,** 213–228.

Favier, N., Chevrot, S. & Komatitsch, D., 2004. Near-field influences on shear wave splitting and traveltime sensitivity kernels, *Geophys. J. Int.,* **156,** 467–482.

Fouch, M.J., Silver, P.G., Bell, D.R. & Lee, J.N., 2004. Small-scale variations in seismic anisotropy near Kimberley South Africa, *Geophys. J. Int.,* **157,** 764–774.

Gibson, R.L. & Ben-Menahem, A., 1991. Elastic wave scattering by anisotropic obstacles: Application to fractured volumes, *J. Geophys. Res.,* **96,** 19 905–19 924.

Helffrich, G., Silver, P. & Given, H., 1994. Shear-wave splitting variation over short spatial scales on continents, *Geophys. J. Int.,* **119,** 561–573.

Hung, S.H., Dahlen, F.A. & Nolet, G., 2000. Fréchet kernels for finite-frequency traveltimes-II. Examples, *Geophys. J. Int.,* **141,** 175–203.

Komatitsch, D. & Tromp, J., 1999. Introduction to the spectral-element method for 3-D seismic wave propagation, *Geophys. J. Int.,* **139,** 806–822.

Komatitsch, D. & Tromp, J., 2002. Spectral-element simulations of global seismic wave propagation-I. Validation, *Geophys. J. Int.,* **149,** 390–412.

Komatitsch, D., Barnes, C. & Tromp, J., 2000. Simulation of anisotropic wave propagation based upon a spectral element method, *Geophysics,* **65**(4), 1251–1260.

Mainprice, D. & Silver, P.G., 1993. Interpretation of SKS-waves using samples from the subcontinental lithosphere, *Phys. Earth planet. Int.,* **78,** 257–280.

Mainprice, D., Barruol, G. & Ben Ismaïl, W., 2000. The seismic anisotropy of the Earth's mantle: From single crystal to polycristal, *Geophys. Monogr.,* **117,** 237–264.

Mensch, T. & Rasolofosaon, P., 1997. Elastic-wave velocities in anisotropic media of arbitrary symmetry—generalization of Thomsen's parameters ϵ, δ and γ, *Geophys. J. Int.,* **128,** 43–64.

Restivo, A. & Helffrich, G., 1999. Teleseismic shear wave splitting measurements in noisy environments, *Geophys. J. Int.,* **137,** 821–830.

Rümpker, G. & Ryberg, T., 2000. New 'Fresnel-zone' estimates for shear-wave splitting observations from finite-difference modeling, *Geophys. Res. Lett.,* **27,** 2005–2008.

Rümpker, G., Tommasi, A. & Kendall, J.M., 1999. Numerical simulations of depth-dependent anisotropy and frequency-dependent wave propagation effects, *J. Geophys. Res.,* **104,** 23 141–23 153.

Saltzer, R.L., Gaherty, J.B. & Jordan, T.H., 2000. How are shear wave splitting measurements affected by variations in the orientation of azimuthal anisotropy with depth?, *Geophys. J. Int.,* **141,** 374–390.

Savage, M.K. & Silver, P.G., 1993. Mantle deformation and tectonics: Constraints from seismic anisotropy in the western United States, *Phys. Earth planet. Int.,* **78,** 207–227.

Silver, P.G., 1996. Seismic anisotropy beneath the continents: Probing the depths of geology, *Ann. Rev. Earth planet. Sci.,* **24,** 385–432.

Silver, P.G. & Chan, W.W., 1991. Shear wave splitting and subcontinental mantle deformation, *J. Geophys. Res.,* **96,** 16 429–16 454.

Vinnik, L., Kosarev, G.L. & Makeyeva, L.I., 1984. Anisotropy of the lithosphere from the observations of *SKS* and *SKKS*, *Proc. Acad. Sci. USSR,* **278,** 1335–1339.

Virieux, J., 1986. *P-SV* wave propagation in heterogeneous media: velocity-stress difference-method, *Geophysics,* **51,** 889–901.

Wolfe, C.J. & Silver, P.G., 1998. Seismic anisotropy of oceanic upper mantle: Shear wave splitting methodologies and observations, *J. Geophys. Res.,* **103,** 749–771.

APPENDIX A: MEASURING SHEAR WAVE SPLITTING PARAMETERS

The most popular technique to measure splitting parameters on *SKS* waves was introduced by Silver & Chan (1991). Most other techniques follow similar principles. We summarize them here and discuss the differences with our approach.

In Silver & Chan (1991), the splitting parameters are determined by finding the optimal inverse splitting operator $\mathbf{\Gamma^{-1}}$, defined by the fast axis direction ϕ_0 and the delay time δt, that minimizes energy on the transverse component. When propagating through an anisotropic layer, the incident shear wave is split into two quasi-shear waves, polarized in the fast and slow directions, that propagate at different velocities and accumulate a delay time δt. Let us define the rotation tensor

$$\mathbf{R} = \begin{pmatrix} \cos\beta & -\sin\beta \\ \sin\beta & \cos\beta \end{pmatrix} \tag{A1}$$

that changes the radial and transverse coordinate system to that defined by the fast and slow directions. The angle β is the angle between the radial and fast directions. Let us also define the delay time operator:

$$\mathbf{D} = \begin{pmatrix} e^{i\omega\delta t/2} & 0 \\ 0 & e^{-i\omega\delta t/2} \end{pmatrix}. \tag{A2}$$

For an incident wave $\mathbf{u_0}$, the displacement $\mathbf{u}$ at the top of the anisotropic layer in the radial and transverse coordinate system is then given by:

$$\mathbf{u}(\omega) = \mathbf{R^{-1}}.\mathbf{D}.\mathbf{R}.\mathbf{u_0}(\omega). \tag{A3}$$

In Silver & Chan (1991), the splitting operator is defined as $\Gamma = \mathbf{D}.\mathbf{R}$. From eq. (A3), noise-free radial and transverse components of an *SKS* wave recorded at the surface can be written in the time domain:

$$u_{\mathrm{R}}(t) = \cos^2\beta u^i_{\mathrm{R}}(t+\delta t/2) + \sin^2\beta u^i_{\mathrm{R}}(t-\delta t/2), \tag{A4}$$

$$u_{\mathrm{T}}(t) = -1/2\sin 2\beta\left[u^i_{\mathrm{R}}(t+\delta t/2) - u^i_{\mathrm{R}}(t-\delta t/2)\right], \tag{A5}$$

where u^i_{R} denotes an incident wave polarized in the radial direction. Inverting eq. (A3), we obtain the seismogram corrected for shear wave splitting:

$$\tilde{\mathbf{u}}(\omega) = \mathbf{R^{-1}}.\mathbf{D^{-1}}.\mathbf{R}.\mathbf{u}(\omega), \tag{A6}$$

which in the time domain gives

$$\begin{aligned}\tilde{u}_{\mathrm{R}}(t) = {} & \cos^2\beta u_{\mathrm{R}}(t-\delta t/2) + \sin^2\beta u_{\mathrm{R}}(t+\delta t/2) \\ & + \frac{1}{2}\sin 2\beta\left[u_{\mathrm{T}}(t+\delta t/2) - u_{\mathrm{T}}(t-\delta t/2)\right]\end{aligned} \tag{A7}$$

and:

$$\begin{aligned}\tilde{u}_{\mathrm{T}}(t) = {} & \frac{1}{2}\sin 2\beta\left[u_{\mathrm{R}}(t+\delta t/2) - u_{\mathrm{R}}(t-\delta t/2)\right] \\ & + \cos^2\beta u_{\mathrm{T}}(t+\delta t/2) + \sin^2\beta u_{\mathrm{T}}(t-\delta t/2).\end{aligned} \tag{A8}$$

Measuring splitting parameters now consists of finding the optimal pair of parameters $(\beta, \delta t)$ that minimizes energy on the transverse component:

$$\begin{aligned}|\tilde{u}_{\mathrm{T}}|^2 = {} & \frac{1}{2}\sin^2 2\beta\left[C_{\mathrm{RR}}(0) - C_{\mathrm{RR}}(\delta t)\right] \\ & + \sin^4\beta C_{\mathrm{TT}}(0) + \cos^4\beta C_{\mathrm{TT}}(0) + \frac{1}{2}\sin^2 2\beta C_{\mathrm{TT}}(\delta t) \\ & + \sin 2\beta\sin^2\beta C_{RT}(\delta t) + \sin 2\beta\cos^2\beta C_{RT}(0) \\ & - \sin 2\beta\sin^2\beta C_{RT}(0) - \sin 2\beta\cos^2\beta C_{RT}(-\delta t),\end{aligned} \tag{A9}$$

where C_{XY} is the correlation function between $X(t)$ and $Y(t)$. Let us define the variable $\tau = \delta t$. The minimum of eq. (A9) is obtained when

$$\frac{\partial|\tilde{u}_{\mathrm{T}}|^2}{\partial\tau} = \frac{\partial|\tilde{u}_{\mathrm{T}}|^2}{\partial\beta} = 0. \tag{A10}$$

The displacement recorded at the surface is contaminated by noise:

$$u_{\mathrm{R}}(t) = u^0_{\mathrm{R}}(t) + n_{\mathrm{R}}(t), \tag{A11}$$

$$u_{\mathrm{T}}(t) = u^0_{\mathrm{T}}(t) + n_{\mathrm{T}}(t). \tag{A12}$$

If we make the assumption that signal and noise are mutually independent, and that noise on the transverse and radial components is uncorrelated, correlation functions are given by:

$$C_{\mathrm{RR}}(\tau) = C^O_{\mathrm{RR}}(\tau) + C_{\mathrm{N_RN_R}}(\tau), \tag{A13}$$

$$C_{\mathrm{TT}}(\tau) = C^O_{\mathrm{TT}}(\tau) + C_{\mathrm{N_TN_T}}(\tau), \tag{A14}$$

$$C_{RT}(\tau) = C^O_{\mathrm{RT}}(\tau), \tag{A15}$$

where

$$C^O_{\mathrm{RR}}(\tau) = \int_{t_1}^{t_2} u^0_{\mathrm{R}}(t+\tau/2)u^0_{\mathrm{R}}(t-\tau/2)\,dt, \tag{A16}$$

$$C^O_{\mathrm{RT}}(\tau) = \int_{t_1}^{t_2} u^0_{\mathrm{R}}(t+\tau/2)u^0_{\mathrm{T}}(t-\tau/2)\,dt, \tag{A17}$$

$$C_{\mathrm{N_RN_R}}(\tau) = \int_{t_1}^{t_2} n_{\mathrm{R}}(t+\tau/2)n_{\mathrm{R}}(t-\tau/2)\,dt, \tag{A18}$$

$$C_{\mathrm{N_TN_T}}(\tau) = \int_{t_1}^{t_2} n_{\mathrm{T}}(t+\tau/2)n_{\mathrm{T}}(t-\tau/2)\,dt. \tag{A19}$$

We can expand eqs (A13), (A14) and (A15) in Taylor series, keeping all terms up to second order:

$$C_{\mathrm{RR}}(\tau) = C^O_{\mathrm{RR}}(0) + C_{\mathrm{N_RN_R}}(0) + \frac{1}{2}\tau^2\partial_{\tau\tau}\left[C^O_{\mathrm{RR}}(0) + C_{\mathrm{N_RN_R}}(0)\right],$$

$$C_{\mathrm{TT}}(\tau) = C^O_{\mathrm{TT}}(0) + C_{\mathrm{N_TN_T}}(0) + \frac{1}{2}\tau^2\partial_{\tau\tau}\left[C^O_{\mathrm{TT}}(0) + C_{\mathrm{N_TN_T}}(0)\right],$$

$$C_{\mathrm{RT}}(\tau) = C^O_{\mathrm{RT}}(0) + \tau\partial_\tau C^O_{\mathrm{RT}}(0) + \frac{1}{2}\tau^2\partial_{\tau\tau}C^O_{\mathrm{RT}}(0).$$

Introducing these expressions in eq. (A10), we get:

$$\begin{aligned}0 = {} & -\frac{1}{2}\tau\sin 2\beta\left[\partial_{\tau\tau}C^0_{\mathrm{RR}}(0) + \partial_{\tau\tau}C_{\mathrm{N_RN_R}}(0)\right] \\ & + \frac{1}{2}\tau\sin 2\beta\left[\partial_{\tau\tau}C^0_{\mathrm{TT}}(0) + \partial_{\tau\tau}C_{\mathrm{N_TN_T}}(0)\right] \\ & + \partial_\tau C^0_{\mathrm{RT}}(0) \\ & + \cos 2\beta\tau\partial_{\tau\tau}C^0_{\mathrm{RT}}(0).\end{aligned} \tag{A20}$$

Eq. (A20) defines a complex non-linear relation between the splitting parameters τ and β and the radial and transverse components of the seismic signal. In general, this relation allows one to determine both parameters from a single seismic record, a clear advantage over measuring splitting intensity, which is a combination of both parameters. However, when the amplitude of the transverse component is small, i.e. when splitting is small either because anisotropy is small or because the polarization of the incoming wave is close to the fast or slow axes direction, $C_{\mathrm{TT}}(0) \sim C_{\mathrm{N_TN_T}}(0)$ and $C_{\mathrm{TT}}(0) \sim C_{\mathrm{N_RN_R}}(0)$, and the parameters β and τ that verify eq. (A20) may be strongly biased. As a result, the technique of Silver & Chan (1991) does not provide reliable estimates of the splitting parameter. This is a well-known limitation that has been quantified by Restivo & Helffrich (1999). They have shown that for signal-to-noise ratios lower than ∼4, this technique gives unreliable measurements. To overcome this problem, Wolfe & Silver (1998) introduced a stacking technique to obtain accurate measurements in noisy environments. However, combining all azimuths into a single measurement procedure becomes more or less equivalent to the multichannel technique introduced by Chevrot (2000). The important difference, however, is that splitting intensity along a single path can be measured robustly and then used directly to image the spatial variations of anisotropy.